On the low frequency boundary of Sun-generated MHD turbulence in the slow solar wind

Bidzina Shergelashvili
in collaboration with Horst Fichtner

Cosmic Rays and the Heliospheric Plasma Environment

12 - 16 September 2011, Ruhr-Universität Bochum, Germany

Based on:
Shergelashvili & Fichtner, 2011, ApJ, Submited

Vainio, Laitinen & Fichtner, 2003, A&A, 407, 713

Outline

Motivation

The model

Results

Conclussions

Motivation (Observations: coronal magnetic field structure)

J.D. Richardson, J.C. Kasper / Journal of Atmospheric and Solar-Terrestrial Physics 70 (2008) 219–225

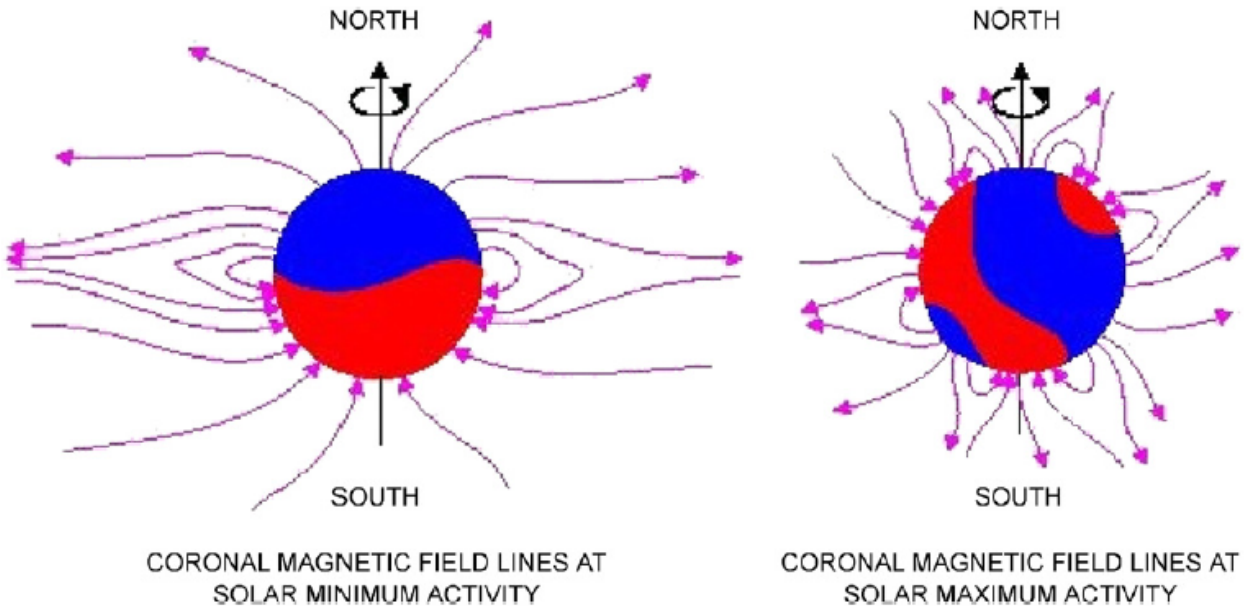

Fig. 1. A schematic diagram showing the change in the solar magnetic field configuration from dipolar with a small current sheet tilt at solar minimum to disordered at solar maximum. Adapted from http://www.sp.ph.ic.ac.uk/~forsyth/reversal.

At the solar minimum the magnetic field has relatively regular structure, while at the maximum it becomes fragmented leading to constraints on the available spatial scales of the wave excitation sources.

Motivation (Observations: solar wind velocity cyclic variability)

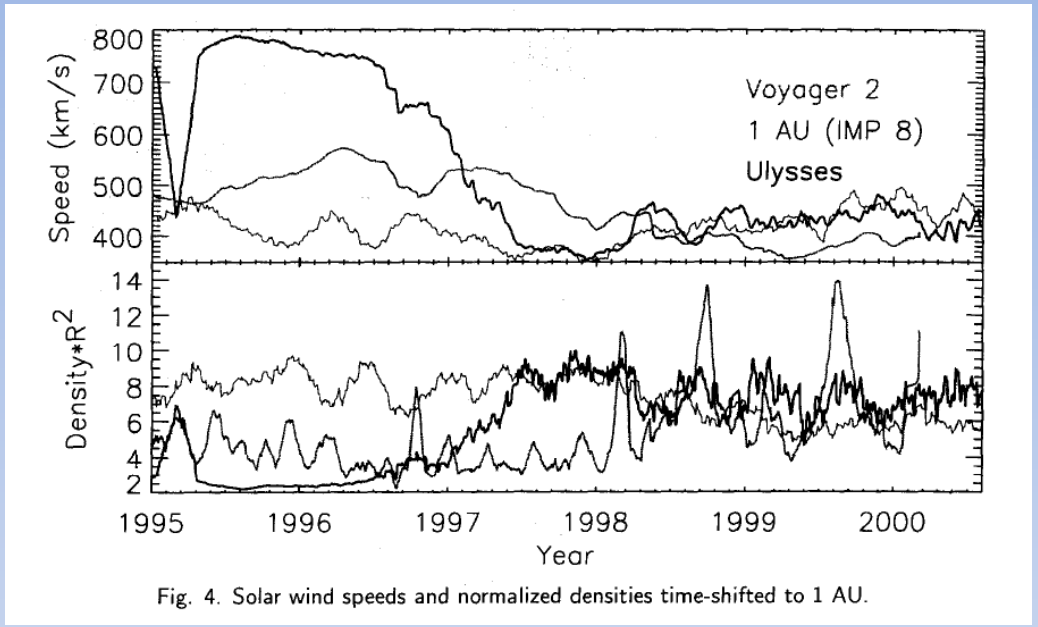

Fig. 4. Solar wind speeds and normalized densities time-shifted to 1 AU.

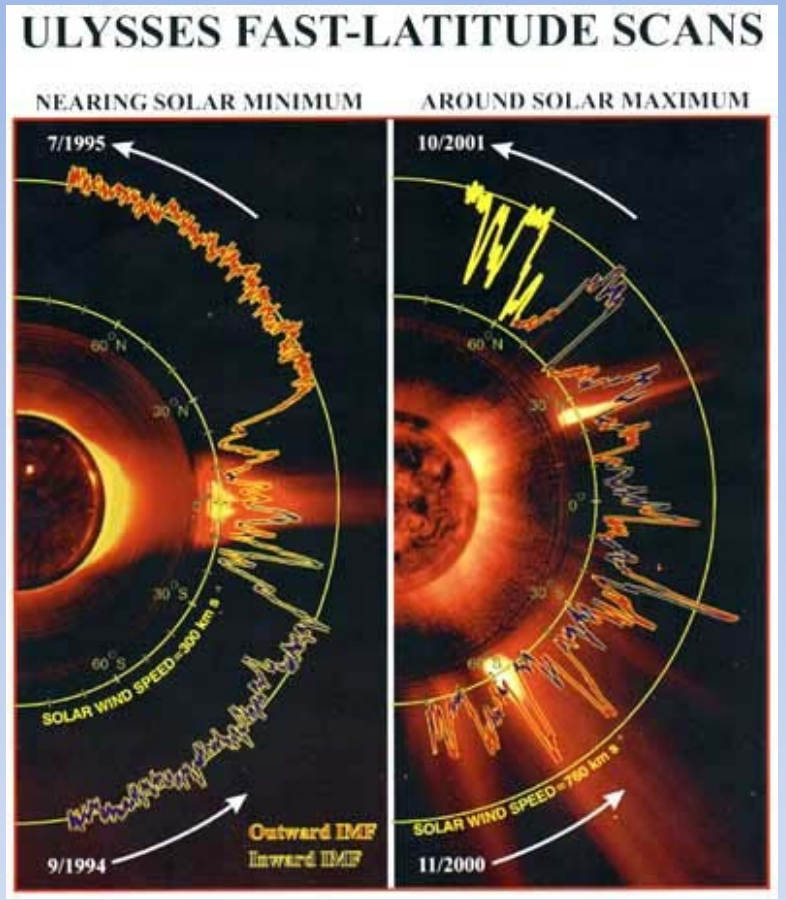

Along with the increasing rate of the magnetic field structure fragmentation the latitudinal area generating the slow solar wind outflow expands significantly , while the polar coronal holes become retreated close to the polar regions. As a result, the velocity gradiends become less pronounced over the wide range of the heliographic latitudes.

Motivation (Observations: solar wind helium abundance)

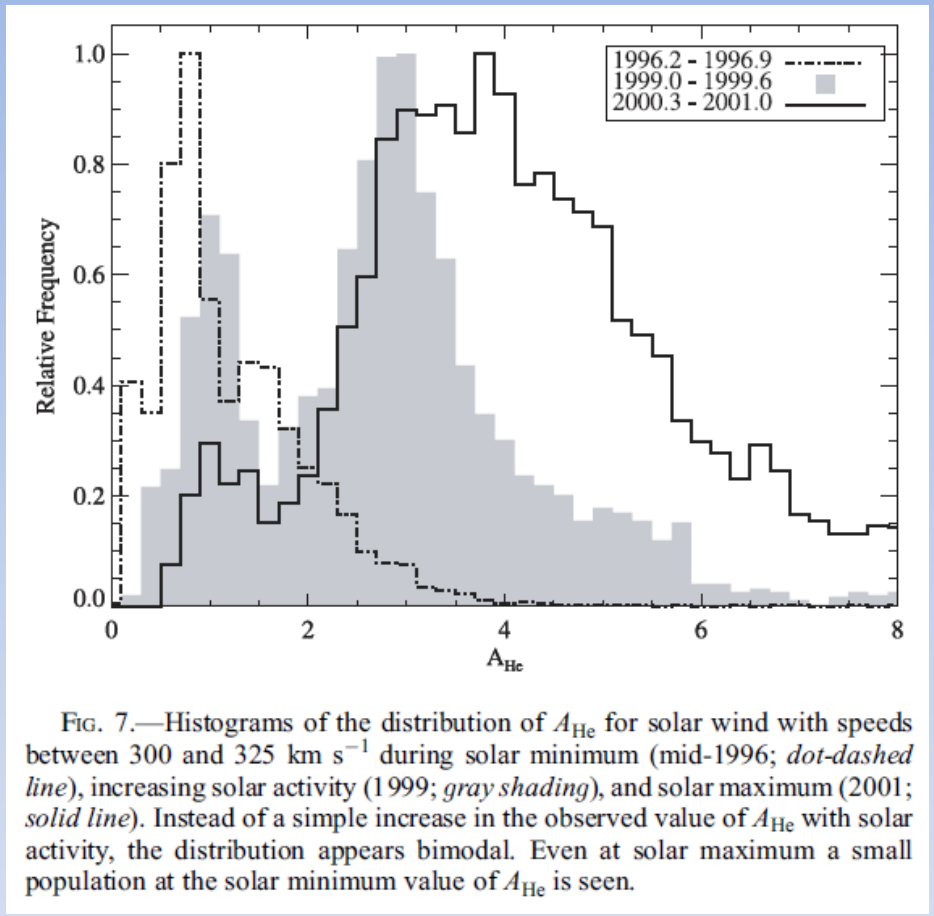

FIG. 7.—Histograms of the distribution of A_{He} for solar wind with speeds between 300 and 325 km s^{-1} during solar minimum (mid-1996; *dot-dashed line*), increasing solar activity (1999; *gray shading*), and solar maximum (2001; *solid line*). Instead of a simple increase in the observed value of A_{He} with solar activity, the distribution appears bimodal. Even at solar maximum a small population at the solar minimum value of A_{He} is seen.

There are two sources of the slow solar wind operating at different stages of solar cycle (Kasper et al., Apj, 2007, 660, 901).

Motivation (Observations: Latitudinal probbility of active region sources)

Liewer, P. C., Neugebauer, M., and Zurbuchen, T., (2004), Solar Phys., **223**, 209

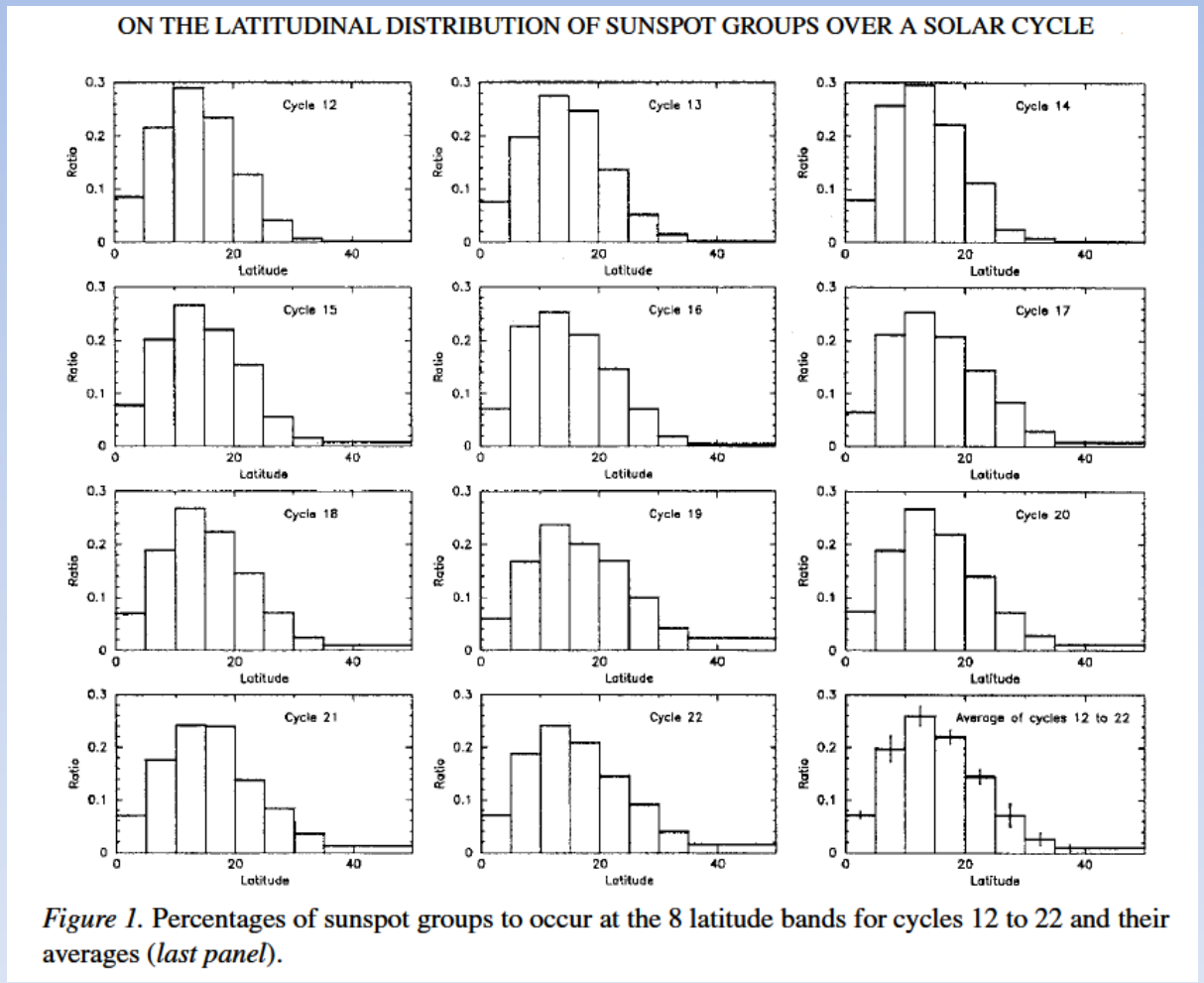

Figure 1. Percentages of sunspot groups to occur at the 8 latitude bands for cycles 12 to 22 and their averages (*last panel*).

$$f(\vartheta) = \frac{\beta^{\kappa}}{\Gamma(\kappa)} \vartheta^{\kappa-1} e^{-\beta\vartheta},$$

$\sigma^2 = \kappa/\beta^2$, $\kappa = 3.99$ and $\beta = 0.258$.

$$\mu = \kappa/\beta$$

$$\psi(\vartheta) = \frac{\int_{\vartheta-\sigma}^{\vartheta+\sigma} f(\vartheta')d\vartheta'}{\max\left\{\int_{\vartheta-\sigma}^{\vartheta+\sigma} f(\vartheta')d\vartheta'\right\}}.$$

Li, K.J., Wang, J.X., Zhan, L.S., Yun, H.S., Liang, H.F., Zhao, H.J., and Gu, X.M., (2003), Sol. Phys., **215**, 99

The model (basic concepts)

- 1D model of the Alfvén wave turbulent heating and acceleration of the solar wind, developed by Vainio, Laitinen, and Fichtner, 2003, A&A, 407, 713, is used as a reference model.

- We update the model by adding the latitudinal variation of the lower frequency boundary of the wave spectrum f_0 , which we claim to be finite due to the fragmentation of the available space for the wave excitation sources.

- We mimic the distribution of the frequency lower boundary of the wave spectrum by imposing upper boundary on the available wavelength in accordance with the typical widths of streamer-like field structures emerged during the cycle.

$$H(x) = \frac{1}{1+e^{-2kx}}, x \in (-\infty, \infty)$$

$$V(\tau, \vartheta) = V_1(\tau) + (800 - V_1(\tau))H(\vartheta - \vartheta_1),$$

$$V_1(\tau) = 400 + 200 \left|\sin\left(\frac{\pi}{11}\tau\right)\right| .$$

$$\vartheta_1 = \pi/12 + (5\pi/18)|\sin(\pi\tau/11)|$$

$$\vartheta_2 = (7\pi/18)|\sin(\pi\tau/11)|$$

$$Sc = \frac{300 - 200|\sin(\frac{\pi}{11}\tau)|}{H(\vartheta_2 - \vartheta)},$$

The model (basic concepts, Fig.1)

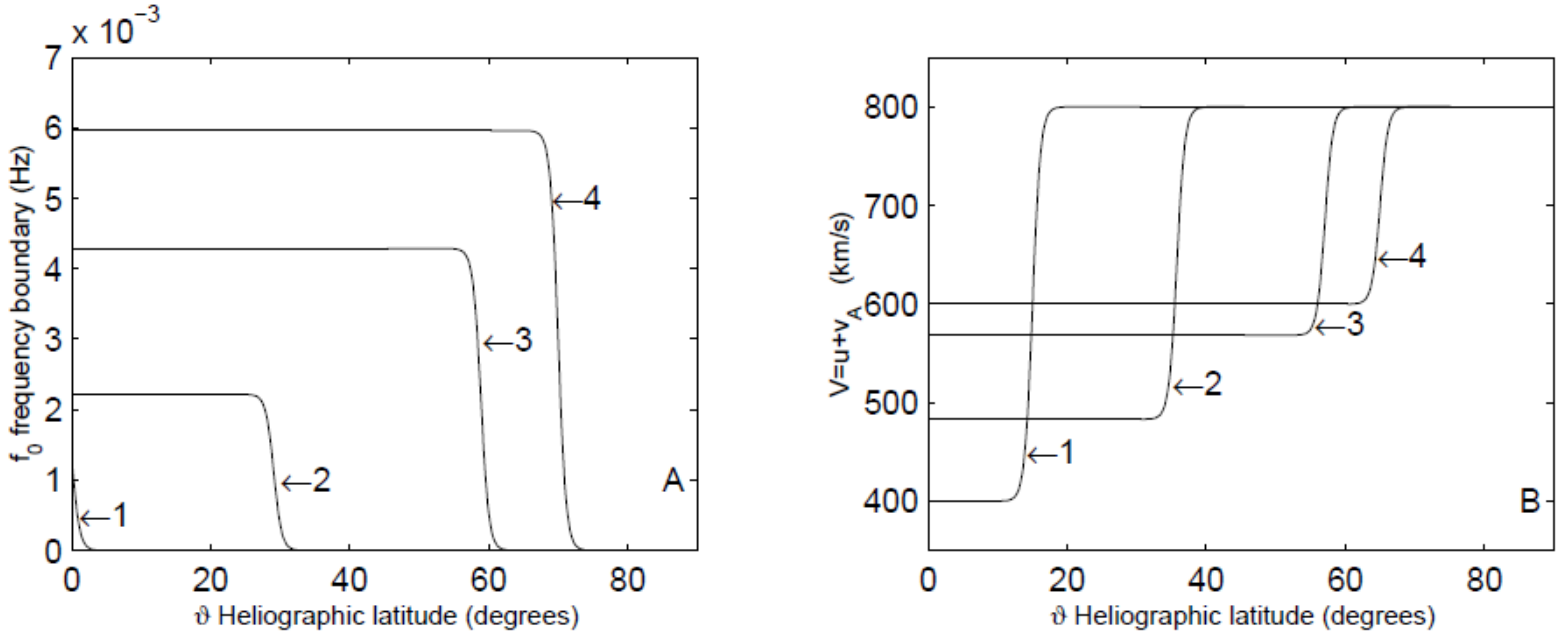

Fig. 1.— Panel A: Modelled latitudinal distribution of the lower boundary of the frequency spectrum. The curves correspond to four different phases of the solar cycle: $\tau = 0, 1.5, 3.5$ and and 5.5 (years counted from minimum activity) labeled 1 to 4, respectively. Panel B: curves of the total speed V vs. latitude. The four curves are shown in the same order as in Panel A.

The model (definitions and equations)

The wave power evolution:

$$\frac{\partial P}{\partial t} + \vec{\nabla} \cdot [(\vec{u} + \vec{v}_A)P] + \frac{P}{2}(\vec{\nabla} \cdot \vec{u}) = -\frac{\partial F}{\partial f}$$

The wave pressure:

$$p_w = \frac{1}{8\pi} \int_{f_0}^{f_H} P \mathrm{d}f.$$

The wave pressure evolution:

$$\frac{\partial p_w}{\partial t} + \vec{\nabla} \cdot [(\vec{u} + \vec{v}_A)p_w] + \frac{p_w}{2}(\vec{\nabla} \cdot \vec{u}) + \frac{Q_w}{2} = 0$$

The wave heating function:

$$Q_w = Q_{w1} + Q_{w2} = \frac{1}{4\pi}\left[F(f_H) - F(f_0)\right] + \frac{(\vec{u} + \vec{v}_A)}{4\pi}\left[P(f_0)\vec{\nabla} f_0 - P(f_H)\vec{\nabla} f_H\right]$$

The model (definitions and equations)

$$F = 2\pi C^2 \frac{v_A}{V} \frac{f^{5/2} P^{3/2}}{B}. \tag{14}$$

The physical quantities in the latter expression are defined by Vainio et al. (2003) as follows:

$$P(f,r) - \frac{P_{\mathrm{WKB}}(f,r)}{1 + [f/f_c(r)]^{2/3}}, \tag{15}$$

to define the wave power $P(f,r)$. Here,

$$P_{\mathrm{WKB}}(f,r) = P(f,r_\odot) \frac{B(r) v_A(r)}{B_\odot v_{A\odot}}, \tag{16}$$

represents the part of the spectral power outside the inertial range where waves follow predominantly WKB behaviour where

$$P(f,r_\odot) = \varepsilon_P \frac{B_\odot^2}{f}, \tag{17}$$

and $f_c(r)$ is the breakpoint frequency at which the Kolmogorov type of the spectrum starts to prevail:

$$\frac{1}{f_c(r)} = 2\pi \varepsilon_P^{1/2} \int_{r_\odot}^{r} \frac{C^2(r') v_A(r')}{V^2} \left(\frac{n_{e\odot}}{n_e(r')} \right)^{1/4} dr' \tag{18}$$

The model (The wave power spectrum)

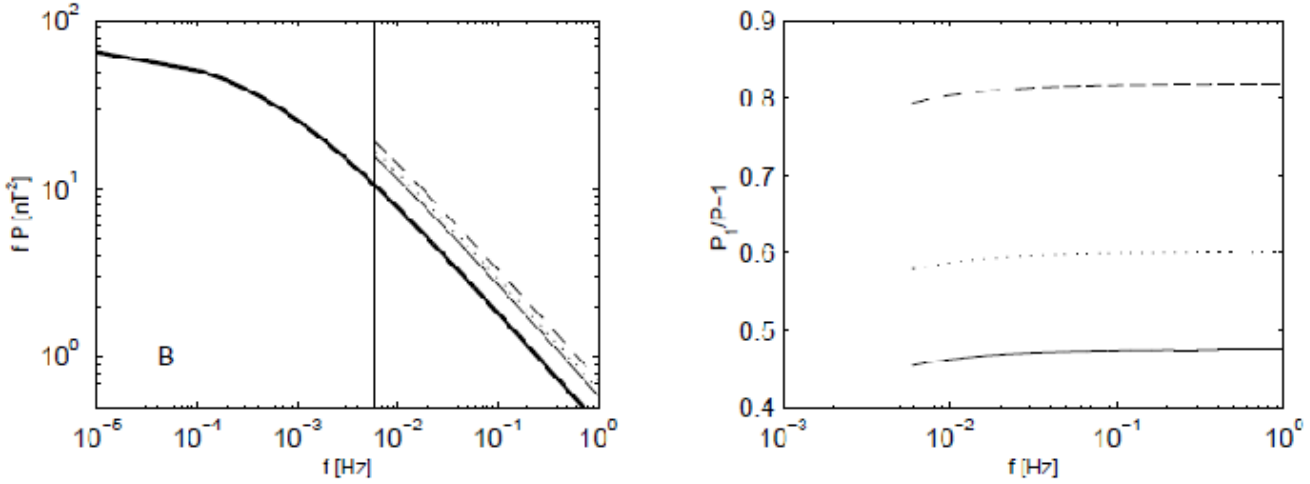

$$\vartheta_1 = 5.1°,\ \vartheta_2 = 13.2° \text{ and } \vartheta_3 = 20°$$

Fig. 2.— Panel A: The wave power spectra (fP) vs. frequencies. The very thick solid line is the complete spectrum of the reference model, which in our model corresponds to the solar minimum. The vertical line marks the cut-off frequency f_0. The three curves to the right of the latter are the new spectra (fP_1), that include the waves from active region sources compensating for losses related to the truncation of the original spectrum, at the different latitudes ϑ_1 (solid line), ϑ_2 (dashed line) and ϑ_3 (dotted line). Panel B: The relative difference $P_1/P - 1$ for the considered three latitudes using corresponding linestyles.

The model (The wave power spectrum)

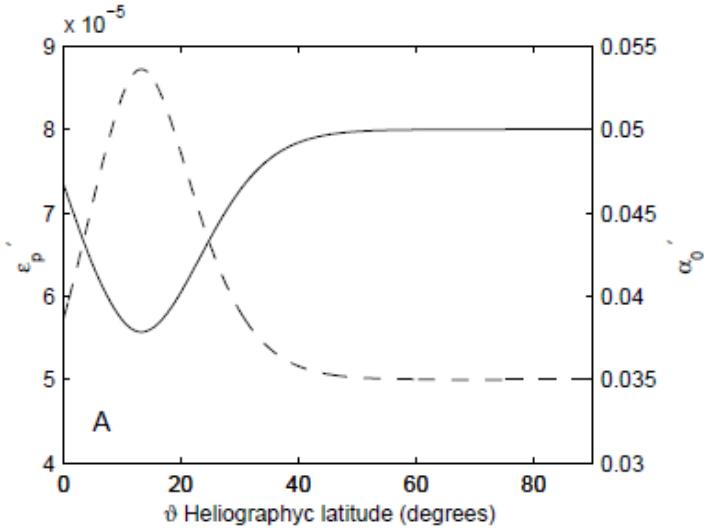

Fig. 5.— The spectral parameter ε'_p (dashed line) and the coefficient of interrelation between outgoing and incoming wave intensities α'_0 (solid line) vs. heliographic latitude.

$$\alpha_1 = \begin{cases} \alpha_0 \left(\frac{r-r_\odot}{9r_\odot}\right) & r_\odot \le r < 10r_\odot \\ \alpha_0 & r \ge 10r_\odot \end{cases}$$

$$C^2(r) = \alpha\alpha_1(r)$$

$$\alpha'(f_0(\vartheta)) = \alpha_0\sqrt{\frac{\varepsilon_{P0}}{\varepsilon'_P}}.$$

$$\varepsilon'_P(f_0(\vartheta)) = \varepsilon_{P0}\left(1 + \psi(\vartheta)\frac{F(f_0(\vartheta), r_m)}{F(f_H, r_m) - P(f_H, r_m)V\left(\frac{df_H}{dr}\right)_{r_m)}}\right)$$

Results (loses in the wave heating rate due to f_0 and compensation by the active region wave sources)

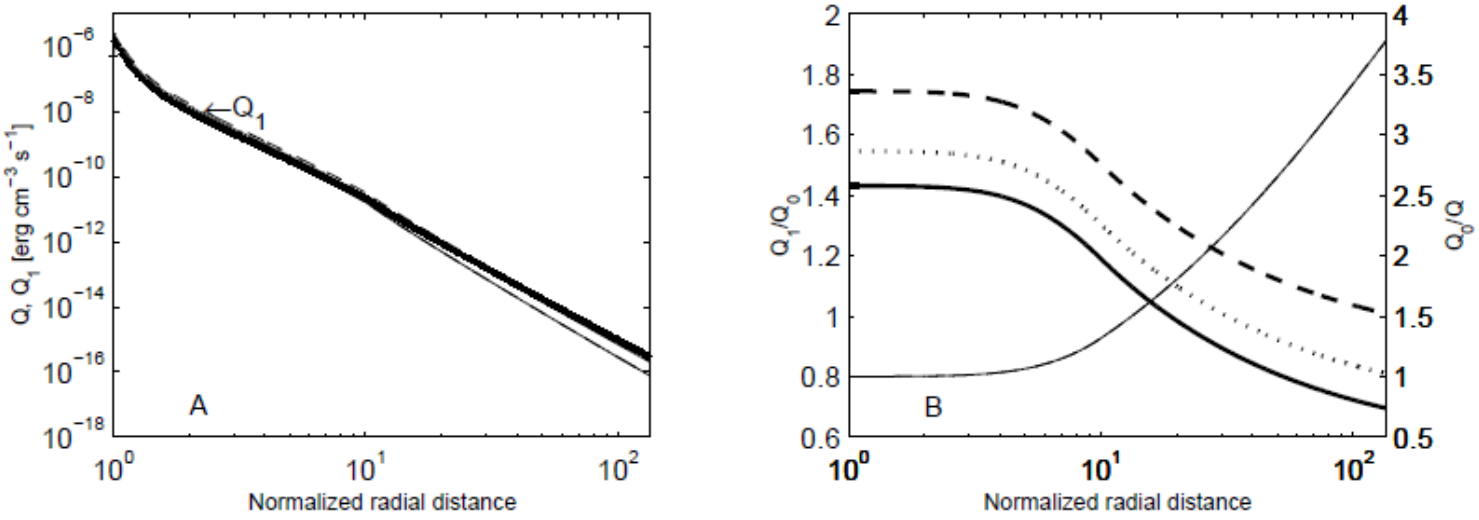

$$\vartheta_1 = 5.1^\circ,\ \vartheta_2 = 13.2^\circ \text{ and } \vartheta_3 = 20^\circ$$

Fig. 3.— Panel A: Calculated heating rates Q_0 (reference model, very thick solid line), Q (modified heating using truncated spectrum for the three different latitudes mentioned in Fig. 3, thin lines) and Q_1 (heating including waves from active regions, dashed line).Panel B: Plots of ratios Q_1/Q_0 (thick lines) and Q_0/Q (thin lines) corresponding to the curves shown in Panel A. The linestyles for Q (thin lines) and Q_1 (thick lines) correspond to the latitudes given in Figure 2.

Results (loses in the wind acceleration rate due to f_0 and compensation by the active region wave sources)

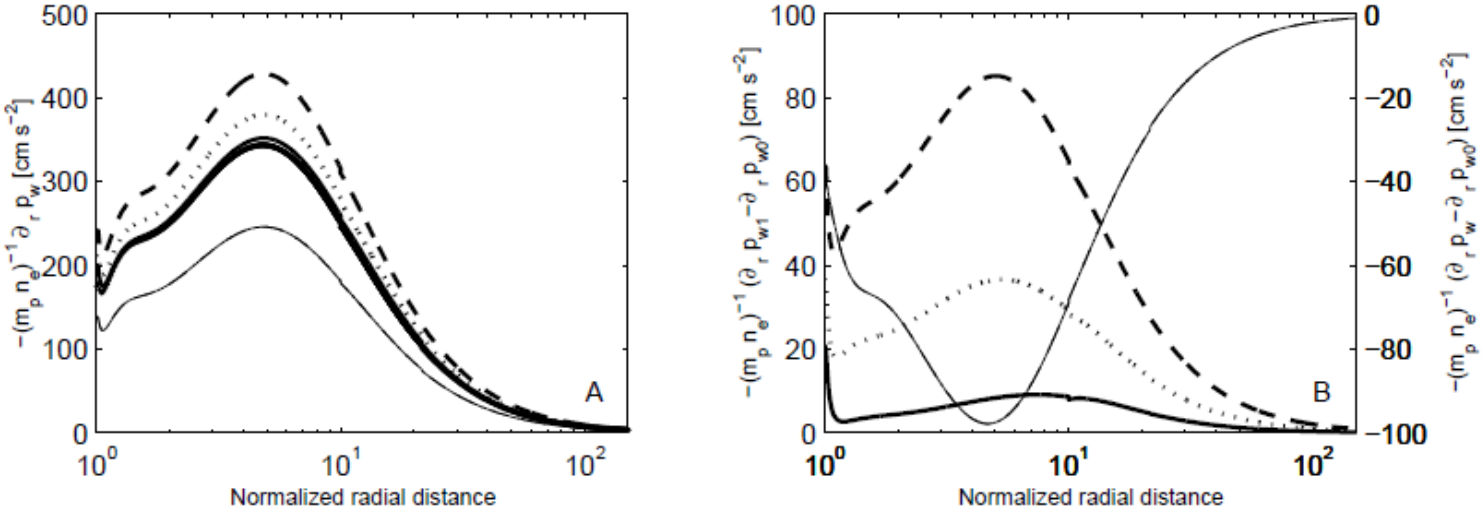

$$\vartheta_1 = 5.1°,\ \vartheta_2 = 13.2° \text{ and } \vartheta_3 = 20°$$

Fig. 4.— Panel A: Calculated wave pressure gradients $-(m_p n_e)^{-1}(\partial p_{w0}/\partial r)$ (very thick solid line), $-(m_p n_e)^{-1}(\partial p_w/\partial r)$ (thin line) and currently $-(m_p n_e)^{-1}(\partial p_{w1}/\partial r)$ (thick lines).Panel B: Plots of the differences $-(m_p n_e)^{-1}(\partial p_{w1}/\partial r - \partial p_{w0}/\partial r)$ (thick lines) and $-(m_p n_e)^{-1}(\partial p_w/\partial r - \partial p_{w0}/\partial r)$ (thin solid line) corresponding to the curves shown in Panel A. The linestyles correspond for p_w (thin solid line) and p_{w1} (thick lines) to the latitudes as in figures 2 and 3.

Conclusions

• In the current work we focused on the basic physical grounds underlying the concept we are addressing. While more extended numerical studies via performing direct numerical simulations will be published elsewhere, here we demonstrate, in general terms, a correspondence of the above-stated modeling with the existing data and modern understanding of the solar wind acceleration scenarios. The lower boundary of the wave frequency domain should be taken into account as a natural parameter!

• most of the indirect measurements of the active region evolution during the solar cycle, like detections of the helium abundance in the solar wind, indicate that multiple processes for slow wind heating and acceleration should operate in the relative proportions at different phases of the solar cycle (Kasper et al. 2007). With the uptrend of the activity cycle the significance of the streamer belt contribution decreases gradually reaching some smaller but finite rates at maximum.

• Contributions from the increasing number of active regions lead another important process to be switched on. At a certain stage this latter process starts to prevail and at solar maximum it mainly contributes to the slow wind dynamics. The resulting magnetic structures as sources of the waves are known as active region sources (Liewer et al. 2004). As a matter of fact, the distribution we have proposed is nothing else than that of active region sources.